ACS Catalysis

pubs.acs.org/acscatalysis

Research Article

Role of Secondary Coordination Sphere Residues in Halogenation Catalysis of Non-heme Iron Enzymes

R. Hunter Wilson, Sourav Chatterjee, Elizabeth R. Smithwick, Joseph J. Dalluge, and Ambika Bhagi-Damodaran*

Cite This: *ACS Catal.* 2022, 12, 10913−10924

Read Online

ACCESS | Metrics & More | Article Recommendations | Supporting Information

ABSTRACT: Chemo- and regio-selective catalysis of the C(sp^3)-H halogenation reaction is a formidable goal in chemical synthesis. 2-Oxoglutarate (2OG)-dependent non-heme iron halogenases catalyze selective chlorination/bromination of C−H bonds and exhibit high sequence and structural similarities with non-heme iron hydroxylases. How the secondary coordination sphere (SCS) of these two enzyme systems differentiate and determine their reactivity is not well understood. In this work, we show that specific positioning of redox-active tyrosine residues in the SCS of non-heme iron halogenases has a huge impact on their structure, function, and reactivity. We discover that a tyrosine residue (F121Y) rationally incorporated to hydrogen bond to iron's chloride ligand in SyrB2 halogenase undergoes post-translational oxidation to dihydroxyphenylalanine (DOPA) physiologically. A combination of spectroscopic, mass-spectrometric, and biochemical studies demonstrate that DOPA modification in SyrB2 renders the enzyme non-functional. Bioinformatic analysis suggests that SyrB2-like halogenases, unlike hydroxylases, have a conserved placement of phenylalanine at position 121 to preclude such unproductive oxidation. Furthermore, molecular dynamics simulations in tandem with experimental demonstration of DOPA incorporation exclusively at position 121 enables us to uniquely identify that an axial-chloro haloferryl isomer is operant in SyrB2. We also identify conserved redox-inactive residues in the SCS of other 2OG-dependent non-heme iron halogenases to avoid DOPA-like unproductive oxidations. Overall, this study demonstrates the importance of the SCS in controlling the structure and enzymatic activity of non-heme iron halogenases and will have significant implications toward the design of small-molecule and protein-based halogenation catalysts.

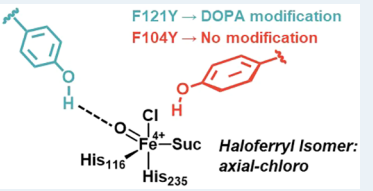

KEYWORDS: *halogenation, DOPA, non-heme iron, 2OG-dependent, O_2 activation*

INTRODUCTION

2OG-dependent non-heme iron enzymes catalyze a diverse range of reactions ranging from epoxidation to stereo-inversion.[1] From natural product biosynthesis to cellular signaling and metabolism, the reactions catalyzed by this superfamily of enzymes serve crucial roles biologically.[2,3] Two subgroups of this superfamily are the hydroxylases and halogenases. Hydroxylases catalyze the insertion of a hydroxyl functional group into unactivated aliphatic C−H bonds whereas halogenases catalyze the insertion of a chloride/bromide functionality into such bonds. The difference in reactivity of the two enzymes is enabled by differences in their iron-binding primary coordination sphere. Hydroxylases bind iron via a 2 His/1 Carboxyl (Asp/Glu) facial triad analogous to halogenases except that in halogenases the carboxyl ligand is replaced by a non-polar Ala or Gly residue.[1,4] This amino acid substitution in halogenases enables the steric and electrostatic accommodation of an iron coordinated halide anion that is essential for halogenation reactivity.[5] Both hydroxylases and halogenases have been suggested to operate via a similar catalytic mechanism (Figure S1).[6,7] Once 2OG, iron, and the substrate are bound to the enzyme, a conformational change is triggered that facilitates molecular oxygen binding to the iron center. Next, oxidative decarboxylation of the 2OG co-substrate results in the cleavage of oxygen's O−O bond and the formation of a high-valent ferryl intermediate (Fe^{4+}=O). The ferryl intermediate abstracts a hydrogen atom from the substrate, resulting in a ferric−hydroxyl (Fe^{3+}−OH) species and a substrate radical. At this point, the mechanisms for the hydroxylases and halogenases diverge. In hydroxylases, the hydroxyl group bound to the iron will "rebound" and combine with the substrate radical to give a hydroxylated product. In halogenases, the protein positions the halide ligand closer to the substrate radical than the hydroxyl ligand. This favors radical combination with the halide ligand resulting in a halogenated product, though a minor hydroxylated product is also possible through hydroxyl rebound.[8−10]

This work focuses on a well-characterized halogenase, SyrB2, which chlorinates/brominates the side-chain methyl group of

Received: February 23, 2022
Revised: July 23, 2022
Published: August 22, 2022

https://doi.org/10.1021/acscatal.2c00954
ACS Catal. 2022, 12, 10913−10924

its substrate Thr.[11,12] Substrate Thr is delivered to the active site of SyrB2 via the partner protein SyrB1's covalently attached phosphopantetheine (Ppt) group.[11] Recent computational work from Kulik and co-workers details the protein−protein interactions needed for entry into the active site.[13] When Thr is substituted with non-native amino acid substrates such as alpha-aminobutyric acid or norvaline, SyrB2 primarily hydroxylates them.[8] These studies and others have demonstrated the importance of SyrB2's interaction with Thr and other amino acid substrates to influence halogenation/hydroxylation reaction outcomes.[8,13−17] While substrate−protein interactions in SyrB2 have been explored, it is unclear how iron's secondary coordination sphere (SCS; amino acid residues that interact with the ligands bound to iron) governs the reaction outcome in SyrB2 and other halogenases. Computational studies in SyrB2 have suggested that a proximal arginine residue, Arg242, may stabilize or isomerize the ferryl intermediate or may act as a proton shuttler, but these hypotheses have yet to be experimentally tested.[18−20] From a broader perspective, although the impact of the SCS on the structure and function of heme iron enzymes have been extensively studied, little is known about how non-heme iron enzymes utilize SCS to control their reactivity.[9,10,21−23] In this work, we investigate the importance of iron's SCS in controlling SyrB2 halogenase's reactivity. Specifically, we rationally incorporate tyrosine residues at 104 and 121 positions in SyrB2 that are capable of H-bonding with iron's aqua and chloride ligands, respectively. Although F121Y residue in SyrB2 undergoes post-translational modification (PTM) to dihydroxyphenylalanine (DOPA), F104Y remains unperturbed. The differential PTM of DOPA residue in the two SyrB2 mutants in tandem with molecular dynamics (MD) simulations confirms the axial-chloro configuration of haloferryl isomer to be operant in SyrB2. Based on further bioinformatic and structural analyses, we conjecture on the nature of protected haloferryl isomers in other 2OG-dependent non-heme iron halogenases. Overall, our studies emphasize the importance of the SCS in controlling catalytic activities of non-heme iron enzymes, particularly halogenases and hydroxylases.

MATERIALS AND METHODS

Plasmid Design and Mutagenesis. SyrB1, SyrB2, SyrB2 mutants, and Sfp were all incorporated into pET-28a(+) vectors. TycF was incorporated into a pET-30b(+) vector. All plasmids are designed with an N-terminal His_6-Tag. Site-directed mutagenesis was performed on the SyrB2 plasmid to form the F104Y and F121Y mutations using the Phusion site-directed mutagenesis kit from Thermo Scientific. The forward and reverse primers (5′ to 3′) for the F104 mutation were: GAGTTCTATCCCAAATATCCGGGCG and TTTGGGATAGAACTCGGTACGCCAG, respectively. The forward and reverse primers (5′ to 3′) for the F121Y mutation were: CACCTACGCCAATGCCTCCGGCA and CATTGGCGAAGGTGTCGGCCTGG, respectively. A three-step denaturation, annealing, and extension protocol was used for both mutants with an annealing temperature of 67.6 °C for F104 and 72.0 °C for F121Y. All PCR experiments were performed using an Axygen MaxyGene II instrument as previously described.[24] All PCR products were transformed into DH5α cells (Thermo Scientific) for plasmid expression. Single mutant DNA sequences were confirmed using Sanger sequencing at the UMN Genomics Center.

Protein Expression. SyrB1, SyrB2, SyrB2 mutants, and Sfp were all expressed using the same method. Plasmids containing the protein sequences were transformed into BL21(DE3) cells (Thermo Scientific) for protein overexpression. An overnight culture (∼50 mL 2XYT broth, 0.05 mg/mL kanamycin) was grown at 37 °C for ∼16 h at 220 rpm. 10 mL of the overnight culture was used to inoculate 1 L cultures (2XYT, 0.05 mg/L kanamycin) in 2.8L baffled flasks. A single drop of Antifoam 204 (Sigma) was added to each culture to aid in oxygen diffusion. Cultures were grown at 37 °C until an OD_{600} of 0.6−0.8 was reached. Cultures were then placed in an ice bath for 15−20 min to cool. Isopropyl β-D-1-thiogalactopyranoside (IPTG, GoldBio) was added to a final concentration of 0.2 mM to induce protein overexpression. After 18 h of shaking at 18 °C, cell pellets were harvested by centrifugation, flash frozen in liquid nitrogen, and stored at −20 °C. Typical yields were ∼8−10 g cell pellet/L culture. Overexpression for TycF followed the same protocol except that [IPTG] = 1 mM and the expression time was 72 h.

Protein Purification. All buffers and solutions described herein were prepared in MilliQ water from a Barnstead GenPure water filtration system (Thermo Scientific) with a resistivity of at least 18.2 MΩ. For all proteins, thawed cell pellets were resuspended in 5 mL wash buffer/g of cells [wash buffer = 50 mM N-(2-hydroxyethyl)piperazine-N′-ethanesulfonic acid (HEPES) (Sigma: Biocertified), 300 mM NaCl (Sigma: BioUltra), and 5 mM imidazole (Sigma: ReagentPlus), pH = 7.5]. Resuspension was supplemented with Pierce Protease Inhibitor, ethylenediaminetetraacetic acid (EDTA)-free tablets (Thermo Scientific). After resuspension, cells were lysed by sonication and centrifuged to remove any non-soluble cell debris (20 000 rpm, 20 min, 4 °C). Supernatant was filtered with 0.43 μm syringe filters and loaded onto a wash-buffer equilibrated 5 mL HisTrapFF column (Cytiva, 2 mL/min binding rate) using an AKTA Start protein purification system (Cytiva). After sample application, the column was washed with 15 CV of wash buffer to elute any non-specific binding proteins. Elution occurred using a linear gradient from 0% to 100% elution buffer (elution buffer = 50 mM HEPES, 100 mM NaCl, 250 mM imidazole, pH = 7.5). For TycF, an isocratic elution was performed by washing the column with 10 CV of 30% elution buffer then 10 CV of 100% elution buffer. Relevant protein fractions, as determined by SDS−PAGE analysis, were pooled. Sfp and TycF were dialyzed against RXN buffer (20 mM HEPES, pH = 7.5) overnight, filtered, concentrated using Amicon Ultra 10 kDa MWCO centrifugal filter units (MilliporeSigma), flash frozen in liquid nitrogen, and stored at −80 °C.

SyrB2 and its mutants were buffer exchanged into RXN buffer three times using Amicon Ultra 30 kDa MWCO centrifugal filter units (MilliporeSigma) after initial immobilized metal affinity chromatography. Concentrated protein was diluted to ∼8 mL with RXN buffer and filtered with 0.22 μm filters prior to loading into a superloop connected to an AKTA Pure protein purification system (Cytiva) for size exclusion chromatography. A HiLoad 26/600 Superdex 200 pg column (Cytiva) was pre-equilibrated with RXN buffer. Protein was then applied and eluted (flow = 1 mL/min) over three injection/elution cycles. Relevant fractions, as determined by SDS−PAGE, were pooled and concentrated in the Amicon Ultra 30 kDa MWCO centrifugal filter units. Protein was aliquoted, flash frozen in liquid nitrogen, and stored at −80 °C until further use. Preparation of SyrB1 after initial immobilized

https://doi.org/10.1021/acscatal.2c00954
ACS Catal. 2022, 12, 10913−10924

metal affinity chromatography is described in the next section. All protein concentrations were determined using the absorbance at 280 nm using molar extinction coefficients from the ProtParam tool.[25]

Ppt and Thr Attachment to SyrB1. After immobilized metal affinity chromatography, SyrB1 was buffer exchanged into RXN buffer three times using Amicon Ultra 50 kDa MWCO centrifugal filter units (MilliporeSigma). To attach the Ppt cofactor, SyrB1 (100 μM) was incubated with coenzyme A (1 mM, Sigma: cofactor for acyl transfer), $MgSO_4$ (5 mM, Sigma: BioReagent), and phosphopantetheinyl transferase Sfp (5 μM) for 90 min at room temperature. The reaction mixture was concentrated using the same centrifugal filter units and then diluted to ∼8 mL with reaction buffer. After filtering, the protein was loaded into the superloop of an AKTA Pure protein purification system. The same elution method as described for the SyrB2 proteins was performed except that the flow rate was adjusted to 0.8 mL/min.

Relevant fractions from size exclusion chromatography were pooled and concentrated using centrifugal filter units. To append threonine to the protein, SyrB1-Ppt (100 μM) was incubated with $MgSO_4$ (5 mM), ATP (10 mM, Sigma: Grade I, ≥99%, from microbial), and L-threonine [10 mM, Sigma: reagent grade, ≥98% (high-performance liquid chromatography (HPLC))] in RXN buffer for 30 min at room temperature. After this step, it is crucial that SyrB1-Ppt-Thr remain at cool temperatures to prevent spontaneous hydrolysis of the thioester bond that links threonine to Ppt-SyrB1. The amino acid-loaded protein was then concentrated using the previous centrifugal filter unit, and buffer exchanged four times with RXN buffer to remove excess reaction components. The protein was aliquoted, flash frozen in liquid nitrogen, and stored at −80 °C.

UV−vis Measurements. All UV−vis measurements were recorded on either a Cary 8454 UV−vis spectrophotometer or a Cary 4000 UV−vis spectrophotometer. Measurements with the Cary 4000 were performed in double beam mode with an S/N ratio of 10 000, a timeout of 0.2 s, and a spectral bandwidth of 2 nm. All spectra were background corrected at 900 nm.

EPR Measurements. All SyrB2 samples (WT and F121Y/DOPA) were prepared at a final concentration of 450 μM in a volume of 280 μL. Samples were transferred to EPR tubes (Wilmad) and frozen in a methanol/dry ice bath followed by a liquid nitrogen bath. Both samples were stored in a liquid nitrogen dewar until use. EPR measurements were performed on a Bruker Elexsys E-500 spectrometer with an E500-T-DU Digital upgrade equipped with an Oxford ESR-910 liquid He cryostat. Following are EPR collection parameters for F121Y/DOPA SyrB2: microwave frequency = 9.6 GHz; microwave power = 1.69 mW; modulation amplitude = 9 G; modulation frequency = 100 kHz; and temperature = 2 K. Following are EPR collection parameters for WT SyrB2: microwave frequency = 9.6 GHz; microwave power = 210 μW; modulation amplitude = 5 G; modulation frequency = 100 kHz; and temperature = 2.5 K.

DOPA Nitration/Oxidation Reaction Assay. The following procedure was adapted from the method of Waite et al.[26] Fresh denaturing sodium acetate buffer [200 mM, 8 M urea (Sigma: BioUltra), pH = 4.5] was prepared. F121Y/DOPA SyrB2 protein was diluted and buffer exchanged into this denaturing buffer three times to remove HEPES. Another solution of 1.41 M $NaNO_2$/0.41 M Na_2MoO_4 (nitration reagent, both Sigma: ACS Reagent) was prepared in MilliQ water. The denatured F121Y/DOPA SyrB2 protein (300 μL) was mixed with 1 equivalent (v/v) of the nitration reagent forming a yellow-colored solution. 1 M NaOH (400 μL) was immediately added to oxidize the nitrated species and form the pink-colored dinitro−quinone complex. The UV−vis spectrum of the reaction was then recorded on a Cary 4000 instrument using the parameters described above.

Native Protein Mass Spectrometry. A fresh solution of 5 mM ammonium acetate, pH = 6.5 (AA, Mallinckrodt: Analytical Reagent) was prepared in MilliQ water. Both WT SyrB2 and F121Y/DOPA SyrB2 were buffer exchanged four times into AA using pre-washed (100 mM NaOH, then AA) 0.5 mL Amicon Ultra 30 kDa MWCO centrifugal filter units (MilliporeSigma). Mass spectral analysis of intact SyrB2 protein(s) in their native state was achieved by direct infusion of aqueous buffer-exchanged solutions of SyrB2 (50 μM protein, 50 μM aqueous NH_4OAc diluted with LC/MS grade water) into a Waters Synapt G2 quadrupole time-of-flight mass spectrometer employing the following instrumental parameters: capillary voltage, 3.0; cone voltage, 30; extraction cone voltage, 5.0; source temperature, 100 °C; desolvation temperature, 350 °C; cone gas flow (L/h), 20; and desolvation gas flow (L/h), 440. Samples were infused at 10 μL/min and mass spectra were acquired in continuum mode over the range m/z 1000 to m/z 3000 with a 0.5 s scan time with the following manual quadrupole profile: mass 1000, dwell time 10, ramp time 20; mass 2000, dwell time 20, ramp time 50; mass 2500. Mass spectra of intact (native state) proteins were deconvoluted employing the Waters MaxEnt 1 algorithm with the Waters MassLynx operating system.

Detection of Pyruvate in the F121Y/DOPA SyrB2 Sample. F121Y/DOPA SyrB2 (500 μM) was incubated with the chelator EDTA (5 mM, Sigma: BioUltra) in 100 mM HEPES buffer (pH = 7.5) for 16 h in an Eppendorf ThermoMixer (300 rpm, 4 °C). The sample was then centrifuged to remove any possible precipitation. All protein was transferred to a pre-washed (100 mM NaOH, then RXN buffer) 0.5 mL Amicon Ultra 10 kDa MWCO centrifugal filter unit and concentrated to ∼75 μL. The protein-free small molecule containing flow-through was then subjected to HPLC analysis. Samples were transferred to deactivated, silanized Waters vials.

HPLC analysis was conducted on a Shimadzu Prominence-i LC-2030C 3D Plus system equipped with a Regis Technologies reverse-phase C18 column (4.60 mm × 250 mm × 5 μm). Separations occurred with a gradient separation at a temperature of 27 °C, an injection volume of 10 μL, and a flow rate of 0.5 mL/min. The separation method is as follows: 0% B to 80% B, 0.0 to 25.0 min; 80% B, 25.0 to 28.0 min; 80% B to 0% B, 28.0 to 30.0 min, where solution A is water and solution B is acetonitrile (both HPLC grade). The absorbance profile at 254 nm was monitored for the HPLC traces. A standard sample was prepared as 1 mM sodium pyruvate in 100 mM HEPES (pH = 7.5).

***In Vitro* DOPA Formation Kinetics Assay.** SyrB2-F121DOPA (100 μM) was incubated with 2OG (10 mM) and NaCl (100 mM) in RXN buffer aerobically in a quartz cuvette (1.0 mL total volume). UV−vis kinetics scans were begun and acquired every 15 min. After the initial scan (0 min), ferrous ammonium sulfate (prepared in 2.5 mM H_2SO_4) was added to the solution to a final concentration of 75 μM and the cuvette solution was thoroughly mixed. All readings

https://doi.org/10.1021/acscatal.2c00954
ACS Catal. 2022, 12, 10913−10924

were collected on a Cary 4000 UV−vis spectrophotometer and performed as described above.

Halogenation Assays. WT SyrB2 or F121Y/DOPA SyrB2 (100 μM) was added to RXN buffer containing NaCl (10 mM) and 2OG (1 mM). For the WT system, ferrous ammonium sulfate (Sigma: BioUltra, in 2.5 mM H_2SO_4) was added to the reaction, and the solution was pipette mixed. SyrB1-Ppt-Thr was added to the RXN to a final concentration of 100 μM, and the RXN was pipette mixed again. The total reaction volume was 200 μL, and all steps so far were performed on ice. One volume equivalent of O_2 saturated buffer was added to the reaction, and each solution was pipette mixed. All reactions were transferred to an Eppendorf ThermoMixer and spun at 300 rpm for 10 min and were then transferred to ice. The reactions were loaded into pre-washed (100 mM NaOH, then RXN buffer) 0.5 mL Amicon Ultra 10 kDa MWCO centrifugal filter units, concentrated to ∼50 μL, then diluted to 500 μL, and concentrated again. This washing step was performed two more times. All centrifugation steps occurred at 4 °C to prevent thioester cleavage. TycF thioesterase (final concentration of 5 μM) was added to each centricon for product cleavage in a final volume of 150 μL. The product cleavage reaction was run for 90 min at 25 °C. The centricon volume was diluted to 400 μL with RXN buffer and the flow-through was collected into deactivated, silanized Waters vials. Three total rounds of dilution and collection were performed to collect all cleaved product. The vials containing ∼1.2 mL of cleaved product in RXN buffer were lyophilized overnight.

The dry product was reconstituted in 160 μL of 100 mM borate buffer (Ricca: analytical grade). 18.5 μL of MilliQ H_2O and 1.5 μL of 5 M NaOH were added to each solution to bring the final pH to 8.5. The derivatization agent, 6-aminoquinolyl-N-hydroxysuccinimidyl carbamate (60 mM in acetonitrile, AQC, Cayman Chemical) was added to a final concentration of 6 mM and a total reaction volume of 200 μL. Reactions were mixed and incubated at room temperature for 10 min. A Waters Acquity UPLC coupled to a Waters triple quadrupole mass spectrometer (Acquity TQD) was used for chromatographic separation and detection of AQC-derivatized amino acids. A Waters CORTECS UPLC C18 column (2.1 mm × 100 mm × 1.6 μm) at 55 °C was used during the following 10 min gradient separation with A: Water (VWR International, Omnisolv LC/MS grade) containing 0.1% formic acid and B: ACN (VWR International, OmniSolv LC/MS grade) containing 0.1% formic acid as two mobile phases at a flow rate of 0.5 mL/min: 1% B, 0 to 1.0 min; 1% B to 13% B, 1.0 to 2.0 min; 13% B to 15% B, 2.0 to 5.5 min; 15% B to 95% B, 5.5. to 6.5 min; 95% B, 6.5 to 7.5 min; 95% B to 1% B, 7.5 to 7.7 min; 1% B, 7.7 to 10 min. The SRM transitions monitored for each analyte are tabulated in Table S1. Dwell time for each transition was 0.01 s. For electrospray ionization tandem mass spectrometry in positive ionization mode, parameters were as follows: capillary, 3.5 kV; cone, 35.0 V; extractor, 3 V; rf lens, 0.3 V; source temperature, 120 °C; desolvation temperature, 350 °C; desolvation flow, 800 L/h; cone gas flow, 20 L/h; low-mass resolution (Q1), 15 V; high-mass resolution (Q1), 15 V; ion energy (Q1), 0.3 V; entrance, −5 V; exit, 1 V; collision energies listed in Table S1; low-mass resolution (Q2), 15 V; high-mass resolution (Q2), 15 V; and ion energy (Q2), 3.5 V.

Bioinformatic Analysis. To observe the sequence conservation position 121, the amino acid sequence for SyrB2 was used as a query for a BLAST search in the non-redundant protein database with an e^{-5} cutoff, resulting in 846 hits. Sequences were aligned using the MUSCLE algorithm and visualized using AliView software. Results were filtered between the halogenases (HXA/G motif, 186 sequences) and hydroxylases (HXD/E motif, 660 sequences). Each of the sequence groups were subjected to cluster analysis using the CD-HIT web server to remove redundant sequences of 90% similarity (resulting in 132 halogenase sequences and 503 hydroxylase sequences). Individual halogenase/hydroxylase sequences were realigned with MUSCLE. LOGOS plots were generated for each cluster using WebLogo (https://weblogo.berkeley.edu/logo.cgi). An identical protocol was executed for the halogenases WelO5, BesD, and AdeV. All files used for bioinformatic analysis are publicly available at: https://github.com/abdlabumn/syrb2-F121DOPA.

MD Simulations of F104Y, F121Y, and F121W SyrB2. The starting structure of WT SyrB2 was taken from the Protein Data Bank (PDB: 2FCT).[5] Missing loops and residues were added using the MODELLER module in UCSF Chimera.[27−31] Hydrogen atoms were added using the H++ web server using a pH of 7.5.[32−34] Using the tleap module in AMBER20, SyrB2 protein was parameterized using the ff19SB force field, 2OG was treated with the generalized amber force field (charges were assigned with antechamber), and iron was treated as a ferrous species.[35−39] The protein was solvated in a 10.0 Å OPC water box, and counterions Na^+ and Cl^- were added to neutralize the system.[40] All mutations were performed by manually editing the input WT PDB files by deleting all atom positions beyond the beta carbon and renaming the residue prior to parameterization with tleap. The protein systems were minimized (solvent first, then protein), gently heated to 300 K, and density was equilibrated for 2 ns. Three independent 250 ns production runs were performed for each mutant system. To maintain the primary coordination sphere about iron, all ligand distances were restrained to within 0.1 Å of their crystallographic distances using a force constant of 100.0 kcal mol^{-1} $Å^{-1}$. Trajectory analyses were performed using CPPTRAJ, where an H-bond donor−acceptor distance cutoff was set to 3.2 Å in the H-bond analysis.[41] Error bars for the analyses were calculated using the standard error over the independent simulations (the standard deviation divided by $\sqrt{3}$).[42] AMBER input files used for SyrB2 MD simulations are available publicly at: https://github.com/abdlabumn/syrb2-F121DOPA.

RESULTS AND DISCUSSION

Observation and Characterization of DOPA Post-translational Modification in F121Y SyrB2. A visual inspection of SyrB2's active site reveals two hydrophobic Phe residues that are ∼4 Å away from iron's ligands (Figure 1A).[5] Specifically, the F104 residue is 3.8 Å from the water ligand and the F121 residue is 3.9 Å away from the chloride ligand. To assess if the hydrophobic nature of these residues was important, tyrosine mutants of both residues, that is F104Y and F121Y SyrB2, were constructed, expressed, and purified. Upon purification, WT SyrB2 and F104Y mutants exhibit no signatures in the visible range of the UV−vis spectrum, implying that both halogenases purify without iron bound to the active site (Figure 1B). In contrast, F121Y SyrB2 purified as a blue-green solution with a λ_{max} at 650 nm (Figure 1B). This blue-green chromophore has been observed in a few non-heme iron proteins previously and has been postulated to originate from a ligand-to-metal charge transfer band (LMCT)

https://doi.org/10.1021/acscatal.2c00954
ACS Catal. 2022, 12, 10913−10924

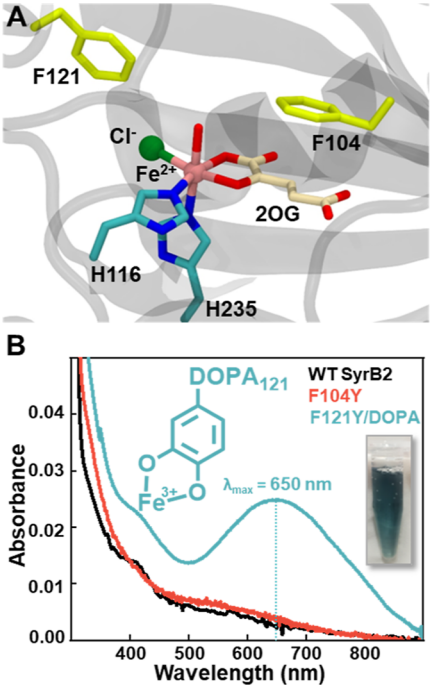

Figure 1. (A) Crystal structure of SyrB2 halogenase (PDB: 2FCT). Prospective residues for mutation are highlighted in yellow. (B) UV−vis spectra of purified SyrB2 WT and mutant proteins (100 μM). A blue-green chromophore is present in the F121Y/DOPA variant, consistent with DOPA incorporation. Shown in inset are the structure of ferric-DOPA and a picture of purified F121Y/DOPA SyrB2 protein.

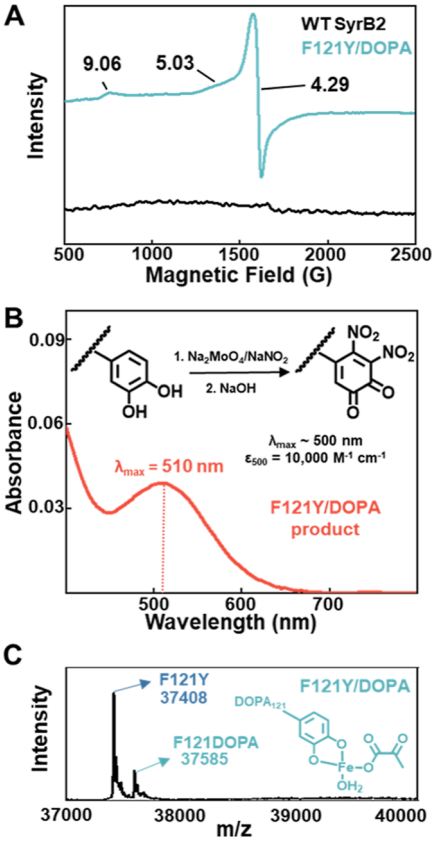

Figure 2. (A) X-band EPR spectra of purified WT SyrB2 and F121Y/DOPA SyrB2. g-values are assigned for features in the F121Y/DOPA spectrum (B) UV−vis spectrum of a DOPA-specific nitration/oxidation reaction product on 20 μM F121Y/DOPA SyrB2 supports ~20% DOPA incorporation into SyrB2. (C) Deconvoluted Native Mass Spectrum of the F121Y/DOPA SyrB2 protein mixture. Two species are observed in the mixture: apo F121Y SyrB2 and F121DOPA SyrB2 with iron and pyruvate bound.

of a DOPA-Fe^{3+} species.[43−47] We hypothesize that such a species has formed from intracellular oxidation of the F121Y mutant and will refer to this SyrB2 variant as F121Y/DOPA.

To investigate the iron oxidation state in F121Y/DOPA, we attempted to oxidize the protein using hydrogen peroxide (Figure S2). Even after incubation with 100 equivalents of peroxide, no shift in the LMCT band was observed, which implies that the iron center is not in the ferrous state. To further characterize the electronic structure of the iron center, we investigated the F121Y/DOPA protein with EPR spectroscopy. The X-band EPR spectrum shows a distinct signal at g ~ 4.29 with additional features at g ~ 5.03 and 9.06 (Figure 2A). The signal at $g \sim 4.29$ is a hallmark of high-spin ferric iron species in a highly orthorhombic environment (E/D = 0.33).[48−51] The broad shoulder at $g \sim 5.03$ and the small peak at $g \sim 9.06$ could be originating from a different Fe^{3+}-bound species in a more rhombic environment (E/D = 0.2). A variation in coordination number of the ferric-DOPA species in F121Y/DOPA could explain the heterogeneity of species in the EPR spectrum. Similar features have been observed in DOPA-modified, non-heme iron (S)-2-hydroxypropylphosphonic acid epoxidase.[45,52] Nevertheless, no EPR signals are observed in the WT SyrB2 spectrum confirming the absence of ferric iron in this protein sample (Figure 2A).

While EPR spectroscopic studies confirm the presence of a high-spin ferric center in the F121Y/DOPA sample, similar signals have been previously observed in a ferric−phenolate complex (i.e., a tyrosinate residue binding to Fe^{3+}) as well.[49] However, high-spin ferric−phenolate species exhibit UV signatures blue-shifted (550 nm) relative to the F121Y/DOPA species (Figure 1B).[48,49] To exclude the possibility of ferric−tyrosinate and confirm the presence of DOPA PTM in the F121Y/DOPA sample, we executed a reaction that specifically targets DOPA amino acids.[26] Nitration/oxidation of the DOPA amino acid results in the formation of a di-nitro-DOPA-quinone species with a distinct UV−vis signature at 500 nm (Figure S3A). We performed this reaction on different concentrations of L-DOPA free amino acid to develop a standard curve, which would quantify the extent of DOPA modification in F121Y/DOPA (Figure S3B). After denaturation of F121Y/DOPA in acidic buffer, the nitration/oxidation reaction was performed and the UV−vis spectrum was recorded (Figure 2B). A peak at 510 nm was present in the product, consistent with other DOPA proteins treated with this method, supporting DOPA modification in F121Y/DOPA SyrB2. Based on the absorbance values (0.04, ε_{500nm}, L-DOPA = 9800 M^{-1} cm^{-1}), we estimate that ~20% of the F121Y/DOPA protein mixture contains the DOPA modification. Thus, F121Y is not fully oxidized to F121DOPA during protein expression. Similar observations were seen in iron-substituted catechol dioxygenase and F208Y ribonucleotide reductase which also purified as a mixture of tyrosine and DOPA containing variants.[43,53] Oxidation of tyrosine to DOPA likely occurs through the formation of the ferryl intermediate. Both hydroxylases and halogenases have evolved to bind their substrates prior to forming the reactive ferryl oxidant.[1,7] Thus,

https://doi.org/10.1021/acscatal.2c00954
ACS Catal. 2022, 12, 10913−10924

any non-productive ferryl formation in the absence of the native substrate likely occurs on a very slow timescale which could explain why only a fraction of F121Y/DOPA exhibits the DOPA modification.

To further characterize the DOPA species, we performed intact native protein mass spectrometry on F121Y/DOPA SyrB2. Representative mass spectra of F121Y/DOPA SyrB2 is illustrated in Figure S4. Algorithmic deconvolution of these peaks reveals the masses of the intact SyrB2 F121Y/DOPA protein (Figure 2C). The first mass at 37408 Da corresponds to the apo F121Y SyrB2 mutant. This mass is lower than expected for F121Y SyrB2 (theoretical mass: 37525 Da). This missing mass (117 Da) can be accounted for by the C-terminal residue, valine, which was cleaved during ionization in the MS experiments. A second less intense peak was found at 37585 Da, which is 177 Da greater than the apo F121Y species. Given the presence of iron and DOPA modification accounts for only 72 Da of mass, an extra 105 Da is left unaccounted for. Because the binding of native ligands 2OG (144 Da) and succinate (116 Da) cannot account for this mass differential, other smaller ligands may be bound to the ferric-DOPA active site. We hypothesized that non-native and smaller (87 Da) pyruvate could be bound to ferric ion in the active site via its alpha-keto functional group.[49] The active site is possibly quite perturbed with the formation of the ferric-DOPA species (F121 is located ~6 Å from the iron center in the WT crystal structure) and it is feasible that the protein's affinity for various ligands has changed. Given the ubiquity of pyruvate in the cellular environment (390 μM), the over-expressed protein would have an abundance of this ligand available to bind.[54] To confirm the presence of pyruvate in the F121Y/DOPA SyrB2 sample, we incubated the protein with the chelator EDTA in order to liberate the small molecule bound to iron and performed HPLC analysis. A peak with an identical retention time to a pyruvate standard is present in the EDTA-treated protein sample, further validating the presence of pyruvate (Figure S5). The rest of the unaccounted mass (18 Da) is explained by an aqua ligand, which is present in the WT crystal structure and numerous other non-heme iron structures.[5] As a control, we subjected the WT SyrB2 protein to an identical mass spectrometric analysis (Figure S6A,B). Unlike F121Y/DOPA SyrB2, only a single discrete population results from deconvolution, which implies that the WT protein purifies with no iron bound. Our EPR analysis further validates this observation (Figure 2A).

To confirm DOPA modification of F121Y SyrB2 occurs during cellular protein expression, we incubated the protein with sub-stoichiometric iron, excess 2OG, and chloride under aerobic conditions. If the LMCT chromophore corresponding to DOPA formed over time (Figure 1B), the process could occur during either protein expression or protein purification. Instead, we observe the formation and conservation of a spectral feature at 520 nm (Figure S7). We ascribe this to a metal-to-ligand charge transfer band between non-bonding electrons of ferrous iron and the antibonding pi orbital of 2OG. This metal-to-ligand charge transfer feature is a common feature across 2OG-dependent hydroxylases and halogenases.[47,55,56] Because DOPA formation did not occur *in vitro*, it is likely this process occurs during protein expression under physiological conditions. Overall, using a combination of spectroscopic, mass-spectrometric, and biochemical studies, we were able to confirm the formation of DOPA PTM in SyrB2 halogenase.

DOPA Modification in SyrB2 Forms an Off-Cycle, Catalytically Inactive Species. Next, we tested the impact of DOPA PTM on the halogenation catalysis of SyrB2. To that end, we developed halogenation assays for SyrB2 with its native substrate, Thr, which is delivered to SyrB2's active site while being covalently bound to the Ppt group of SyrB1. Chlorinated, hydroxylated (minor product), or unreacted threonine were liberated from SyrB1 after incubation with TycF thioesterase.[57] These products were first derivatized with 6-aminoquinolyl-N-hydroxysuccinimidyl carbamate (AQC) and then analyzed by reversed-phase UPLC/multiple-reaction-monitoring-MS/MS (UPLC-MRM-MS/MS) for detection. WT-SyrB2, when subjected to the halogenation assay, reveals AQC-Cl-Thr as the major product, eluting slightly after the unreacted AQC-Thr (Figure 3A). Isotopic ratios of

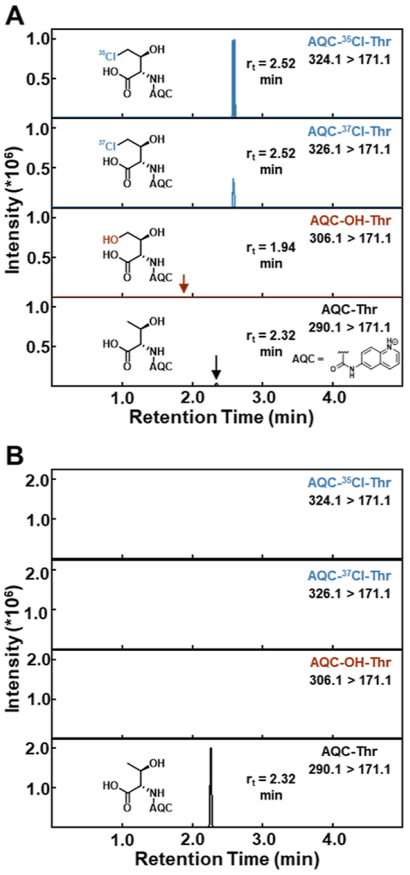

Figure 3. UPLC-MRM-MS/MS chromatograms of the halogenation reaction products for (A) WT and (B) F121Y/DOPA SyrB2 proteins. Reactions using the F121Y/DOPA protein result in no halogenated or hydroxylated products. Mass transitions for each unique analyte are given in the top right corner of each chromatogram.

AQC-^{35}Cl-Thr to AQC-^{37}Cl-Thr were shown to be 3:1, consistent with the natural abundance of chlorine, and providing validation to the identity of chlorinated Thr (Figure S8). The AQC-OH-Thr minor product was also observed, eluting prior to the unreacted AQC-Thr, though with much less intensity than AQC-Cl-Thr. F121Y/DOPA SyrB2, on the other hand, when subjected to similar halogenation assays, showed no chlorinated or hydroxylated products (Figures 3B, S9, and S10). The only analyte observed corresponds to the unreacted Thr substrate (Figures 3B, S9, and S10). Although a low-intensity peak is present close to the noise at 2.52 min in

https://doi.org/10.1021/acscatal.2c00954
ACS Catal. 2022, 12, 10913−10924

the AQC-^{35}Cl-Thr channel, no such peak is seen at the same elution time in the AQC-^{37}Cl-Thr channel suggesting that no chlorinated product was formed. Even in the presence of ten equivalents of ascorbate, no products were observed (Figure S10). With these observations, we postulate that the ferric-DOPA SyrB2 species is a catalytically inactive, off-cycle species. We hypothesize that the modification of tyrosine to DOPA itself is not necessarily the reason why F121Y/DOPA is catalytically inactive. It is the binding of ferric iron by the catecholate group of DOPA that results in an enzymatic species that is not part of the overall catalytic cycle. The DOPA121 is possibly bound to the ferric iron in a bidentate fashion which would result in large distortions in the active site because F121 is located ~6 Å away from iron in the WT active site. To test this hypothesis, we performed UV−vis titration of chloride into F121Y/DOPA SyrB2 and observed no perturbation in the LMCT band alluding to the fact that the DOPA121 residue is binding in a position where chloride would bind or that distortion of the active site prevents chloride binding (Figure S11). Furthermore, it is unclear whether both histidine ligands would still be bound to ferric iron, as they would be needed for proper iron positioning in the active site for native activity. Saturation of coordination sites by DOPA121 would also prevent cofactors such as 2OG and oxygen from binding to the iron site. Occupancy of coordination sites by pyruvate, as shown in our MS studies, would also exacerbate this problem. Overall, the sequestration of ferric iron by the modified DOPA residue abolishes any catalytic activity of SyrB2.

Bioinformatic Analysis Reveals a Conserved Phenylalanine at Position 121 in SyrB2-like Halogenases but Not SyrB2-like Hydroxylases. While we have shown that F121 residue plays a significant role in preventing unproductive oxidation in SyrB2, we wanted to assess the impact of this residue across similar proteins. Using the SyrB2 sequence, we performed a BLAST analysis and sorted hits into hydroxylases (HXD/E motif) or halogenases (HXA/G motif). After removing redundant hits, 635 protein sequences were aligned, and LOGOS plots were generated (Figure 4A). For SyrB2-like hydroxylases (n = 503), the prominent amino acid in position 121 is a redox-active tyrosine. On the other hand, in SyrB2-like halogenases (n = 132), a redox-inactive phenylalanine at position 121 is strongly conserved in 97% of the aligned sequences. Because mutation of phenylalanine to tyrosine at this position in SyrB2 has led to an off-cycle species, it is intriguing that the SyrB2-like hydroxylases have evolved to have a redox-active tyrosine proximal to the reactive iron center. We believe the differential residue conservation at position 121 for hydroxylases and halogenases is due to the isomeric flexibility of the reactive ferryl intermediate (Figure 4B).[7,13,17,18,55,58−64] Two isomers of the ferryl intermediate are plausible for hydroxylases. One describes a trigonal bipyramidal structure with the oxo ligand in the axial position. The other is best described as a distorted five-coordinate structure with the Asp/Glu ligand and the oxo ligand in the equatorial plane.[63] Due to the presence of a third amino acid residue (Asp/Glu) coordinating to the iron center, hydroxylases may exert better control over ferryl isomerization. Even if a tyrosine ligand were present in the hydroxylase active site, so long as it is not proximal to the oxo ligand of the ferryl intermediate, unproductive oxidation to DOPA would not occur. In halogenases, Glu or Asp in the facial triad is replaced by Ala or Gly. This replacement sterically and electrostatically

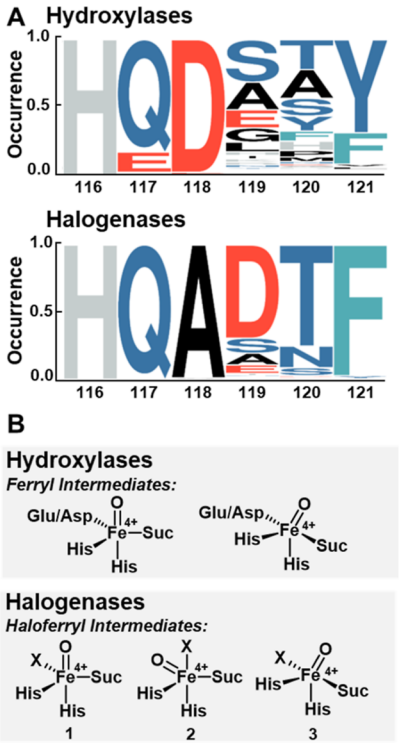

Figure 4. (A) LOGOS plots displaying sequence conservations for homologues of SyrB2 for positions 116−121 in hydroxylases (top, n = 503) and halogenases (bottom, n = 132). In halogenases, phenylalanine is strongly conserved at position 121. (B) Potential reactive ferryl intermediates in hydroxylases and halogenases. X = halide and Suc = succinate.

accommodates halide bound to the iron center. As a consequence, the protein sacrifices control over ferryl isomerization. Three different isomers for the haloferryl intermediate have been proposed for halogenase systems (Figure 4B). One is analogous to hydroxylases and exists as trigonal bipyramidal structure with the oxo ligand in the axial position (**1**). Another isomer is structurally similar to **1** but swaps the positions of the oxo and halide ligands such that the halide ligand is in the axial position (**2**). The last isomer is best described as a distorted five-coordinate structure, with both the oxo and halide ligands occupying equatorial positions (**3**). Given this flexibility, any one of these intermediates could be operant across the 2OG-dependent halogenase enzymes. Because haloferryl intermediates exist in the timescales of seconds,[14] halogenases must prevent a non-productive isomer from damaging the protein or leading to an unreactive enzyme intermediate. Evolution of the redox-inactive phenylalanine residue at position 121, therefore, prevents an unproductive oxidation from occurring, maintains catalytic activity, and allows SyrB2-like halogenases to align a productive ferryl isomer for its halogenation function. We should note that 3% of the aligned SyrB2-like halogenase sequences (Figure 4A) contain a Tyr residue at 121 position and belong to the phytanoyl-CoA dioxygenase family assigned to *Moorea producens*, *Hyella patelloides*, *Alienimonas chondri*, and *Alienimonas californiensis* bacterial species. These outlier sequences are intriguing and merit further examination into how these enzymes are able to avoid Tyr121's unproductive oxidation, or if they even possibly contain a post-translationally modified DOPA residue.

https://doi.org/10.1021/acscatal.2c00954
ACS Catal. 2022, 12, 10913−10924

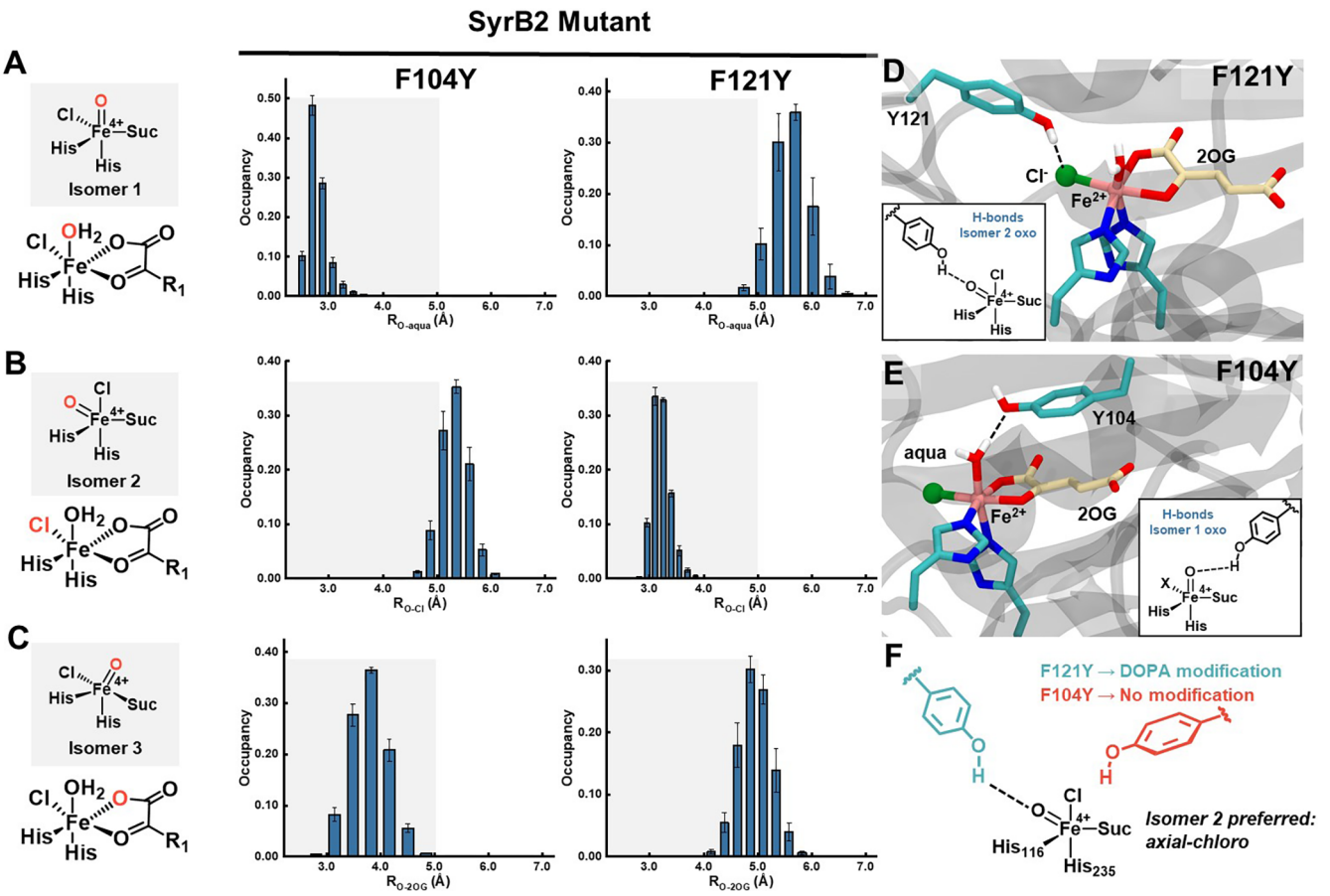

Figure 5. Monitored distance distributions from the MD simulations involving F104Y and F121Y SyrB2 mutants. (A) First row monitors the distance between the hydroxyl oxygen of Tyr and the oxygen atom of the aqua ligand. (B) Row two monitors the distance between the hydroxyl oxygen of Tyr and the halide ligand. (C) Row three monitors the distance between the hydroxyl oxygen of Tyr and the coordinating oxygen of the carboxylate group of 2OG. The iron-bound ligand in red coincides with the position of the oxo ligand for each haloferryl isomer depicted. Shaded regions indicate reactive distances between the oxo ligand and tyrosine (<5.0 Å). The y-axis (occupancy) represents fraction of the simulation where a given distance is observed. F121Y samples distances proximal to the halide ligand, whereas F104Y samples distances proximal to the aqua ligand. (D) MD simulations sample a frequent H-bond between the chloride ligand and F121Y SyrB2, which would be the location of the oxo ligand in an equatorial haloferryl isomer. (E) MD simulations show a highly-sampled H-bond between F104Y SyrB2 and the resting-state aqua ligand, which is the location of the oxo ligand in an axial haloferryl isomer. Although Y104 acts as an H-bond acceptor in this simulation, it is entirely feasible for the donor−acceptor relationship to reverse upon formation of the haloferryl intermediate. (F) DOPA formation occurs only in the F121Y mutant revealing the identity of the haloferryl isomer in SyrB2. R1 = $(CH_2)_2COO^-$ and Suc = succinate.

Engineered Tyrosine Probe for Haloferryl Isomer Identity in SyrB2. While our bioinformatic analysis revealed the function of F121 in SyrB2-like halogenases, we were still intrigued by the preferential PTM of tyrosine in F121Y SyrB2 and not in F104Y SyrB2. Given their proximity to the iron center of SyrB2, both tyrosine residues would be susceptible to further oxidation to DOPA. This led us to hypothesize that a specific haloferryl isomer (Figure 4B) is responsible for this preferential PTM. Specifically, Tyr104 and Tyr121 act as spatially constrained probes for the operant haloferryl isomer in SyrB2. To screen possible reactive configurations, MD simulations were performed on the individual SyrB2 F → Y mutants. These simulations were performed in the absence of a substrate to best mimic SyrB2 under the physiological conditions in which it was expressed. By monitoring distances between the hydroxyl groups of the tyrosine mutants and the ligands that correspond to the locations of the putative oxo ligand in isomers **1**−**3**, as well as H-bonding interactions, we could observe which isomer is poised for reaction with each tyrosine mutant. For DOPA formation to occur in SyrB2, the hydroxyl group of the tyrosine residue must be proximal to the oxo ligand of the haloferryl intermediate. This enables the intermediate to initiate the required H-atom abstraction reaction (Scheme S1).[65] Thus, if a tyrosine residue samples distances proximal (≤5 Å)[16] to individual ligands in the primary coordination sphere (which represent putative locations for a specific haloferryl isomer), then the identity of the operant haloferryl isomer responsible for the oxidation can be resolved. To that end, distance distribution histograms were produced from the distances sampled over the course of three, independent MD simulations for each SyrB2 mutant (Figure 5A−C). Positions of the aqua, chloride, and the 2OG-carboxylate ligands coincide with the position of the oxo ligand in isomers **1**, **2**, and **3**, respectively. In F104Y SyrB2, the tyrosine samples more proximal distances to the axial aqua ligand (2.4−3.4 Å) as compared to either the equatorial chloride ligand (4.5−6.0 Å) or equatorial carboxylate ligand (3.0−5.0 Å). This suggests that F104Y would be spatially primed to react with the axial oxo ligand present in haloferryl isomer **1**. Simulations of F121Y SyrB2 create a different distribution pattern. F121Y favors distances closer to the equatorial chloride ligand (2.9−3.7 Å) than either the axial

https://doi.org/10.1021/acscatal.2c00954
ACS Catal. 2022, 12, 10913−10924

aqua ligand (4.7−6.7 Å) or the equatorial carboxylate ligand (4.2−5.7 Å) (Figure 5A−C). Given this, it appears that F121Y samples configurations amenable to reacting with an equatorial oxo ligand from haloferryl isomer **2**. Both F104Y and F121Y SyrB2 mutants sample reactive distance configurations farther from the carboxylate ligand, which implies that haloferryl isomer **3** would likely not be the reactive isomer for DOPA formation (Figure 5A−C). Next, we sampled H-bonding between the hydroxyl group of Tyr 121 and 104 for various isomeric forms and the ligands coordinated to the iron center (Figure 5D,E). In F121Y SyrB2, an H-bond between the chloride ligand and the hydroxyl group of Y121 was frequently sampled (30% of simulation time), suggesting that F121Y would be primed to react with haloferryl isomer **2** (Figure 5D). For F104Y SyrB2, an H-bond between the aqua ligand and the tyrosine was consistently sampled (70% of simulation time), suggesting that F104Y would favor reaction with haloferryl isomer **1** (Figure 5E). No H-bonds were observed between either F104Y or F121Y and the carboxylate ligand. We note that H-bonding between Tyr and the oxo ligand of the reactive haloferryl intermediate is a crucial first step for H-atom abstraction and DOPA formation. This rules out isomer **3** as the operant haloferryl intermediate conformation. Haloferryl isomer **2**, as compared to the others, best fulfills the geometric criteria for performing H-atom abstraction and DOPA formation on Y121 (Figure 5B,D). Ultimately, these MD studies in tandem with experimental demonstration of DOPA incorporation exclusively at position 121 (Figure 1B) uniquely identifies the haloferryl isomer responsible for DOPA formation in SyrB2 as isomer **2** (axial chloro, Figure 5F). Although the DOPA formation in the F121Y mutant proceeds in the absence of the native SyrB1-Ppt-Thr substrate, these results hold significance for SyrB2's native catalysis. Previous spectroscopic and computational studies have suggested that a combination of haloferryl isomers **1**, **2**, and **3** could be catalytically relavent.[13−15,18,58,64] Our DOPA formation studies in conjunction with MD simulations lends support for isomer **2**'s role in native SyrB2 halogenation catalysis.

We have shown that the placement of tyrosine residues in the SCS can act as a probe for haloferryl intermediates via formation of DOPA. Although tyrosine has been adequate for this purpose, we wanted to investigate if other redox-active amino acids would show the same type of oxidation modification. Tryptophan residues have been shown to undergo an oxidative PTM to form 5-hydroxytrptophan in other non-heme iron enzymes.[44,66] To test the viability of Trp as an isomeric probe, we performed MD simulations of a F121W mutant and monitored the distance distributions between the reactive C5 atom of W121 and the primary coordination sphere atoms of iron (Figure S12). With the same trend as F121Y SyrB2, F121W SyrB2 samples distances closer to the halide ligand (∼4.2 Å) than the aqua ligand (∼5.5 Å). The F121W mutant also samples proximal distances to the iron center itself.[16] This observation, in combination with the analogous F121Y distance patterns with the primary coordination sphere, lead us to believe Trp could also operate as a probe for haloferryl isomer identity via post-translational oxidation.

Conservation of Redox-Inactive SCS Residues across Various Non-heme Iron Halogenases. Because SyrB2 possesses a strongly conserved Phe at position 121 to prevent oxidation with haloferryl isomer **2**, we investigated if other halogenases contained similar redox-inactive residues in their active sites to prevent an unproductive reaction with a haloferryl intermediate. We focused our analysis on the halogenases WelO5, BesD, and AdeV whose activities have been thoroughly characterized and structures resolved by X-ray crystallography.[9,10,67,68] We assessed the crystal structures for putative hydrophobic residues and performed an analogous bioinformatic analysis for residue conservation as we did with SyrB2. For WelO5 halogenase, two residues were identified: Phe169 and Phe276 (Figure S13A). Phe169 resides in the same position as Phe121 in SyrB2 (+5 from the lower numbered iron-coordinating His residue) and is positioned away from the iron center. Although the static crystal structure suggests it may not have a catalytic role, it is feasible for a side-chain rotation to occur about the $C_\alpha-C_\beta$ bond, which would bring Phe169 proximal to the chloride ligand. Furthermore, Phe169 is considerably more conserved in WelO5-like halogenases than in their hydroxylase counterparts, suggesting a role that expands beyond a purely structural one (Figure S13B). Another residue, Phe276, is present in the active site and is positioned proximal to the aqua ligand. Both Phe169 and Phe276 exhibit >80% conservation in WelO5-like halogenases. Placement of redox-inactive Phe in positions proximal to chloro/aqua ligands in WelO5 could prevent a non-productive reaction with haloferryl intermediates. Specifically, detailed computational studies on WelO5 have suggested that haloferryl isomers **2** and **3** are best positioned to perform regio- and stereo-selective halogenation at the C13 position of substrate 12-*epi*-fisherindole U.[64] We note that redox-inactive SCS Phe276 residue positions itself to protect the haloferryl isomer **2**'s oxo ligand ($R_{O\text{-}F276}$ = 3.8 Å) but resides beyond reactive distances of isomer **3**'s oxo ligand ($R_{O\text{-}F276}$ = 5.8 Å) (Figure S16B,C). Phe169 although positioned away from the active site could rotate about the $C_\alpha-C_\beta$ bond during the reaction to protect haloferryl isomers and prevent their non-productive reactions. In BesD halogenase, a hydrophobic residue, Leu197, resides ∼5.0 Å away from the iron center and in an axial position above the equatorial plane defined by the primary coordination sphere (Figure S14A). Leu197 is well-conserved in BesD-like halogenases, with other redox-inactive residues present in BesD-like hydroxylases (Figure S14B). This positioning and residue conservation implies that Leu197 could prevent unproductive oxidation by the axial oxo ligand of haloferryl isomer **1** in BesD-like enzymes. The use of haloferryl isomer **1** in BesD for regio- and stereo-selective halogenation has been previously supported via MD simulations and quantum chemical calculations.[64] Redox-inactive SCS residue Leu197 located proximal to the oxo ligand in BesD ($R_{O\text{-}L197}$ = 3.7 Å) may prevent protein's self-reaction with haloferryl isomer **1** (Figure S16D). Similar to BesD halogenase, AdeV halogenase contains a redox-inactive residue lying in an axial position above the equatorial plane, Phe271 (Figure S15A). This residue resides proximal to the iron-bound aqua ligand which would be the putative position of the oxo ligand in haloferryl isomer **1**. When assessing the conservation of Phe271, it appears to be very well conserved across AdeV-like halogenases as well as other oxygenase counterparts (Figure S15B). This observation suggests that Phe271 may preclude unproductive oxidations when haloferryl isomer **1** forms to perform the halogenation reaction in AdeV. Overall, our experimental and computational results suggest that non-heme iron halogenases contain redox-inactive residues proximal to their iron centers to prevent self-reaction with haloferryl species.

https://doi.org/10.1021/acscatal.2c00954
ACS Catal. 2022, 12, 10913−10924

CONCLUSIONS

We show that the incorporation of a redox-active tyrosine residue at position 121 in SyrB2 results in a PTM to DOPA. This DOPA residue binds ferric iron with high affinity and results in a catalytically inactive, off-cycle enzymatic species. The ferric-DOPA species likely forms as a result of an unproductive oxidation in F121Y-SyrB2 (Scheme S1). F121Y can form an H-bond to the oxo ligand, which may be an initial reactive configuration, but the formation of DOPA must be initiated by an H-atom abstraction. After H-atom abstraction of the hydroxyl group of Y121, the newly formed hydroxyl group on the iron center will rebound and incorporate into the ring structure, eventually forming DOPA121. This residue can become deprotonated and bind ferric iron from the cellular environment, forming the blue-green chromophore we observe upon purification of this protein (Figure 1B). We emphasize that the formation of F121DOPA occurs during the expression of the F121Y mutant and is a substrate (SyrB1-Ppt-Thr) uncoupled process. Should the substrate be present in the F121Y SyrB2 active site, it will likely compete with Y121 for H-atom abstraction. To avoid unproductive, protein-deactivating oxidations, SyrB2-like halogenases tend to keep redox-inactive residues in their SCS, especially in position 121. The placement of redox-inactive residues in the halogenases is especially important due to multiple isomers of ferryl intermediates, as compared to the hydroxylases. Additionally, DOPA formation exclusively at position 121 uniquely identifies an axial-chloro haloferryl intermediate is operant in SyrB2. We have identified several redox-inactive residues across a diverse range of halogenases that may serve a similar function as F121 in SyrB2. Mutation of these residues to redox-active Tyr (or Trp), and subsequent post-translational hydroxylation, could probe the active haloferryl isomer in those halogenases. These findings also hint toward a rational design strategy that could be employed toward identifying the operant haloferryl isomer in non-heme iron enzymes and needs to be further explored experimentally for other halogenases. Finally, our results forecast that placement of redox-active residues can result in catalytically non-functional enzymes and will benefit researchers attempting to engineer non-heme iron enzymes for non-native functions.[69−72]

ASSOCIATED CONTENT

Supporting Information

The Supporting Information is available free of charge at https://pubs.acs.org/doi/10.1021/acscatal.2c00954.

Halogenase/hydroxylase reaction depiction; observed MRM transitions; UV−vis oxidation experiment spectra; DOPA oxidation UV−vis spectra and standard curve; convoluted and deconvoluted MS spectra for WT and F121Y/DOPA SyrB2; pyruvate detection HPLC traces; in vitro F121Y oxidation spectra; UPLC-MRM chromatograms for halogenation assays; Trp MD distance distribution histograms;WelO5, BesD, and AdeV bioinformatic and structural analyses; and energy minimized structures of WelO5 and BesD with their native substrates (PDF)

AUTHOR INFORMATION

Corresponding Author

Ambika Bhagi-Damodaran − *Department of Chemistry, University of Minnesota, Minneapolis, Minnesota 55455, United States;* orcid.org/0000-0002-4901-074X; Email: ambikab@umn.edu

Authors

R. Hunter Wilson − *Department of Chemistry, University of Minnesota, Minneapolis, Minnesota 55455, United States*

Sourav Chatterjee − *Department of Chemistry, University of Minnesota, Minneapolis, Minnesota 55455, United States*

Elizabeth R. Smithwick − *Department of Chemistry, University of Minnesota, Minneapolis, Minnesota 55455, United States*

Joseph J. Dalluge − *Department of Chemistry, University of Minnesota, Minneapolis, Minnesota 55455, United States*

Complete contact information is available at: https://pubs.acs.org/10.1021/acscatal.2c00954

Author Contributions

A.B.D conceived the idea and supervised the project. R.H.W. designed and synthesized the proteins and performed the various biochemical and analytical studies on them. R.H.W., S.C., E.R.S., and J.J.D. designed and performed the UPLC-MRM-MS/MS-based halogenation assay. R.H.W. and E.R.S. performed bioinformatic studies. R.H.W. performed MD simulations. R.H.W. and A.B.D. wrote the manuscript with contributions from all authors. All authors have given approval to the final version of the manuscript.

Funding

R.H.W. and E.R.S. acknowledge the support of the National Institute of Health Chemical Biology Training grant (T32GM132029). This work was supported by the Regents of the University of Minnesota and National Science Foundation CLP and CBET (grant #2046527).

Notes

The authors declare no competing financial interest.

ACKNOWLEDGMENTS

The authors would like to thank Dr. Rahul Banerjee and Prof. John Lipscomb for their productive discussion on EPR experiments. We also thank Prof. William Pomerantz and Noelle Olsen for sodium molybdate dihydrate for the DOPA nitration/oxidation assays. Authors thank Profs. Bollinger and Krebs (Penn State) for SyrB1, SyrB2, and Sfp plasmids and Prof. Blaskus (Harvard) for TycF plasmid.

ABBREVIATIONS

2OG	2-oxoglutarate
SCS	secondary coordination sphere
DOPA	dihydroxyphenylalanine
LMCT	ligand-to-metal charge transfer
Ppt	phosphopantetheine
AQC	6-aminoquinolyl-N-hydroxysuccinimidyl carbamate

REFERENCES

(1) Kal, S.; Que, L. Dioxygen Activation by Nonheme Iron Enzymes with the 2-His-1-Carboxylate Facial Triad That Generate High-Valent Oxoiron Oxidants. *JBIC, J. Biol. Inorg. Chem.* **2017**, *22*, 339−365.

(2) Lee, H.-J.; Lloyd, M. D.; Harlos, K.; Clifton, I. J.; Baldwin, J. E.; Schofield, C. J. Kinetic and crystallographic studies on deacetoxycephalosporin C synthase (DAOCS). *J. Mol. Biol.* **2001**, *308*, 937−948.

(3) Hirsilä, M.; Koivunen, P.; Günzler, V.; Kivirikko, K. I.; Myllyharju, J. Characterization of the Human Prolyl 4-Hydroxylases

That Modify the Hypoxia-Inducible Factor. *J. Biol. Chem.* **2003**, *278*, 30772−30780.
(4) Hegg, E. L.; Jr, L. Q. The 2-His-1-Carboxylate Facial Triad - An Emerging Structural Motif in Mononuclear Non-Heme Iron(II) Enzymes. *Eur. J. Biochem.* **1997**, *250*, 625−629.
(5) Blasiak, L. C.; Vaillancourt, F. H.; Walsh, C. T.; Drennan, C. L. Crystal Structure of the Non-Haem Iron Halogenase SyrB2 in Syringomycin Biosynthesis. *Nature* **2006**, *440*, 368−371.
(6) Solomon, E. I.; Goudarzi, S.; Sutherlin, K. D. O2 Activation by Non-Heme Iron Enzymes. *Biochemistry* **2016**, *55*, 6363−6374.
(7) Solomon, E. I.; DeWeese, D. E.; Babicz, J. T. Mechanisms of O2 Activation by Mononuclear Non-Heme Iron Enzymes. *Biochemistry* **2021**, *60*, 3497−3506.
(8) Matthews, M. L.; Neumann, C. S.; Miles, L. A.; Grove, T. L.; Booker, S. J.; Krebs, C.; Walsh, C. T.; Bollinger, J. M. Substrate Positioning Controls the Partition between Halogenation and Hydroxylation in the Aliphatic Halogenase, SyrB2. *Proc. Natl. Acad. Sci. U.S.A.* **2009**, *106*, 17723−17728.
(9) Mitchell, A. J.; Zhu, Q.; Maggiolo, A. O.; Ananth, N. R.; Hillwig, M. L.; Liu, X.; Boal, A. K. Structural Basis for Halogenation by Iron- and 2-Oxo-Glutarate-Dependent Enzyme WelO5. *Nat. Chem. Biol.* **2016**, *12*, 636−640.
(10) Neugebauer, M. E.; Sumida, K. H.; Pelton, J. G.; McMurry, J. L.; Marchand, J. A.; Chang, M. C. Y. A Family of Radical Halogenases for the Engineering of Amino-Acid-Based Products. *Nat. Chem. Biol.* **2019**, *15*, 1009−1016.
(11) Vaillancourt, F. H.; Yin, J.; Walsh, C. T. SyrB2 in syringomycin E biosynthesis is a nonheme Fe II α-ketoglutarate- and O 2 -dependent halogenase. *Proc. Natl. Acad. Sci. U.S.A.* **2005**, *102*, 10111−10116.
(12) Vaillancourt, F. H.; Vosburg, D. A.; Walsh, C. T. Dichlorination and Bromination of a Threonyl-S-Carrier Protein by the Non-Heme FeII Halogenase SyrB2. *ChemBioChem* **2006**, *7*, 748−752.
(13) Mehmood, R.; Qi, H. W.; Steeves, A. H.; Kulik, H. J. The Protein's Role in Substrate Positioning and Reactivity for Biosynthetic Enzyme Complexes: The Case of SyrB2/SyrB1. *ACS Catal.* **2019**, *9*, 4930−4943.
(14) Matthews, M. L.; Krest, C. M.; Barr, E. W.; Vaillancourt, F. H.; Walsh, C. T.; Green, M. T.; Krebs, C.; Bollinger, J. M. Substrate-Triggered Formation and Remarkable Stability of the C−H Bond-Cleaving Chloroferryl Intermediate in the Aliphatic Halogenase, SyrB2. *Biochemistry* **2009**, *48*, 4331−4343.
(15) Kulik, H. J.; Drennan, C. L. Substrate Placement Influences Reactivity in Non-Heme Fe(II) Halogenases and Hydroxylases. *J. Biol. Chem.* **2013**, *288*, 11233−11241.
(16) Martinie, R. J.; Livada, J.; Chang, W.; Green, M. T.; Krebs, C.; Bollinger, J. M.; Silakov, A. Experimental Correlation of Substrate Position with Reaction Outcome in the Aliphatic Halogenase, SyrB2. *J. Am. Chem. Soc.* **2015**, *137*, 6912−6919.
(17) Rugg, G.; M. Senn, H. Formation and structure of the ferryl [Fe·O] intermediate in the non-haem iron halogenase SyrB2: classical and QM/MM modelling agree. *Phys. Chem. Chem. Phys.* **2017**, *19*, 30107−30119.
(18) Huang, J.; Li, C.; Wang, B.; Sharon, D. A.; Wu, W.; Shaik, S. Selective Chlorination of Substrates by the Halogenase SyrB2 Is Controlled by the Protein According to a Combined Quantum Mechanics/Molecular Mechanics and Molecular Dynamics Study. *ACS Catal.* **2016**, *6*, 2694−2704.
(19) Pandian, S.; A. Vincent, M.; H. Hillier, I.; A. Burton, N. Why does the enzyme SyrB2 chlorinate, but does not hydroxylate, saturated hydrocarbons? A density functional theory (DFT) study. *Dalton Trans.* **2009**, *0*, 6201−6207.
(20) Borowski, T.; Noack, H.; Radoń, M.; Zych, K.; Siegbahn, P. E. M. Mechanism of Selective Halogenation by SyrB2: A Computational Study. *J. Am. Chem. Soc.* **2010**, *132*, 12887−12898.
(21) Zhang, X.; Wang, Z.; Gao, J.; Liu, W. Chlorination versus Hydroxylation Selectivity Mediated by the Non-Heme Iron Halogenase WelO5. *Phys. Chem. Chem. Phys.* **2020**, *22*, 8699−8712.
(22) Bhagi-Damodaran, A.; Reed, J. H.; Zhu, Q.; Shi, Y.; Hosseinzadeh, P.; Sandoval, B. A.; Harnden, K. A.; Wang, S.; Sponholtz, M. R.; Mirts, E. N.; Dwaraknath, S.; Zhang, Y.; Moënne-Loccoz, P.; Lu, Y. Heme Redox Potentials Hold the Key to Reactivity Differences between Nitric Oxide Reductase and Heme-Copper Oxidase. *Proc. Natl. Acad. Sci. U.S.A.* **2018**, *115*, 6195−6200.
(23) Bhagi-Damodaran, A.; Petrik, I. D.; Marshall, N. M.; Robinson, H.; Lu, Y. Systematic Tuning of Heme Redox Potentials and Its Effects on O2 Reduction Rates in a Designed Oxidase in Myoglobin. *J. Am. Chem. Soc.* **2014**, *136*, 11882−11885.
(24) Sanyal, R.; Bhagi-Damodaran, A. An enzymatic method for precise oxygen affinity measurements over nanomolar-to-millimolar concentration regime. *J. Biol. Inorg. Chem.* **2020**, *25*, 181−186.
(25) Gasteiger, E.; Hoogland, C.; Gattiker, A.; Duvaud, S.; Wilkins, M. R.; Appel, R. D.; Bairoch, A. Protein Identification and Analysis Tools on the ExPASy Server. In *The Proteomics Protocols Handbook*; Walker, J. M., Ed.; Humana Press: Totowa, NJ, 2005, pp 571−607.
(26) Waite, J. H.; Benedict, C. V. Assay of Dihydroxyphenylalanine (Dopa) in Invertebrate Structural Proteins. *Methods Enzymol.* **1984**, *107*, 397−413.
(27) Eswar, N.; Webb, B.; Marti-Renom, M. A.; Madhusudhan, M. s.; Eramian, D.; Shen, M.; Pieper, U.; Sali, A. Comparative Protein Structure Modeling Using Modeller. *Curr. Protoc. Bioinforma.* **2006**, *15*, 561−5630.
(28) Martí-Renom, M. A.; Stuart, A. C.; Fiser, A.; Sánchez, R.; Melo, F.; Šali, A. Comparative Protein Structure Modeling of Genes and Genomes. *Annu. Rev. Biophys. Biomol. Struct.* **2000**, *29*, 291−325.
(29) Šali, A.; Blundell, T. L. Comparative Protein Modelling by Satisfaction of Spatial Restraints. *J. Mol. Biol.* **1993**, *234*, 779−815.
(30) Fiser, A.; Do, R. K. G.; Šali, A. Modeling of Loops in Protein Structures. *Protein Sci.* **2000**, *9*, 1753−1773.
(31) Pettersen, E. F.; Goddard, T. D.; Huang, C. C.; Couch, G. S.; Greenblatt, D. M.; Meng, E. C.; Ferrin, T. E. UCSF Chimera?A visualization system for exploratory research and analysis. *J. Comput. Chem.* **2004**, *25*, 1605−1612.
(32) Anandakrishnan, R.; Aguilar, B.; Onufriev, A. V. H++ 3.0: Automating PK Prediction and the Preparation of Biomolecular Structures for Atomistic Molecular Modeling and Simulations. *Nucleic Acids Res.* **2012**, *40*, W537−W541.
(33) Myers, J.; Grothaus, G.; Narayanan, S.; Onufriev, A. A Simple Clustering Algorithm Can Be Accurate Enough for Use in Calculations of PKs in Macromolecules. *Proteins: Struct., Funct., Bioinf.* **2006**, *63*, 928−938.
(34) Gordon, J. C.; Myers, J. B.; Folta, T.; Shoja, V.; Heath, L. S.; Onufriev, A. H++: a server for estimating pKas and adding missing hydrogens to macromolecules. *Nucleic Acids Res.* **2005**, *33*, W368−W371.
(35) Case, D. A. *AMBER*; University of California, 2020.
(36) Tian, C.; Kasavajhala, K.; Belfon, K. A. A.; Raguette, L.; Huang, H.; Migues, A. N.; Bickel, J.; Wang, Y.; Pincay, J.; Wu, Q.; Simmerling, C. Ff19SB: Amino-Acid-Specific Protein Backbone Parameters Trained against Quantum Mechanics Energy Surfaces in Solution. *J. Chem. Theory Comput.* **2020**, *16*, 528−552.
(37) Wang, J.; Wolf, R. M.; Caldwell, J. W.; Kollman, P. A.; Case, D. A. Development and Testing of a General Amber Force Field. *J. Comput. Chem.* **2004**, *25*, 1157−1174.
(38) Li, Z.; Song, L. F.; Li, P.; Merz, K. M. Systematic Parametrization of Divalent Metal Ions for the OPC3, OPC, TIP3P-FB, and TIP4P-FB Water Models. *J. Chem. Theory Comput.* **2020**, *16*, 4429−4442.
(39) Wang, J.; Wang, W.; Kollman, P. A.; Case, D. A. Automatic Atom Type and Bond Type Perception in Molecular Mechanical Calculations. *J. Mol. Graphics Modell.* **2006**, *25*, 247−260.
(40) Izadi, S.; Anandakrishnan, R.; Onufriev, A. V. Building Water Models: A Different Approach. *J. Phys. Chem. Lett.* **2014**, *5*, 3863−3871.
(41) Roe, D. R.; Cheatham, T. E. PTRAJ and CPPTRAJ: Software for Processing and Analysis of Molecular Dynamics Trajectory Data. *J. Chem. Theory Comput.* **2013**, *9*, 3084−3095.

https://doi.org/10.1021/acscatal.2c00954
ACS Catal. 2022, 12, 10913−10924

(42) Nicholls, A. Confidence Limits, Error Bars and Method Comparison in Molecular Modeling. Part 1: The Calculation of Confidence Intervals. *J. Comput.-Aided Mol. Des.* **2014**, *28*, 887−918.
(43) Farquhar, E. R.; Emerson, J. P.; Koehntop, K. D.; Reynolds, M. F.; Trmčić, M.; Que, L. In vivo self-hydroxylation of an iron-substituted manganese-dependent extradiol cleaving catechol dioxygenase. *JBIC, J. Biol. Inorg. Chem.* **2011**, *16*, 589−597.
(44) Liu, A.; Ho, R. Y. N.; Que, L.; Ryle, M. J.; Phinney, B. S.; Hausinger, R. P. Alternative Reactivity of an α-Ketoglutarate-Dependent Iron(II) Oxygenase: Enzyme Self-Hydroxylation. *J. Am. Chem. Soc.* **2001**, *123*, 5126−5127.
(45) Liu, P.; Mehn, M. P.; Yan, F.; Zhao, Z.; Que, L.; Liu, H. Oxygenase Activity in the Self-Hydroxylation of (S)-2-Hydroxypropylphosphonic Acid Epoxidase Involved in Fosfomycin Biosynthesis. *J. Am. Chem. Soc.* **2004**, *126*, 10306−10312.
(46) Ryle, M. J.; Koehntop, K. D.; Liu, A.; Que, L.; Hausinger, R. P. Interconversion of two oxidized forms of taurine/α-ketoglutarate dioxygenase, a non-heme iron hydroxylase: Evidence for bicarbonate binding. *Proc. Natl. Acad. Sci. U.S.A.* **2003**, *100*, 3790−3795.
(47) Solomon, E. I.; Brunold, T. C.; Davis, M. I.; Kemsley, J. N.; Lee, S.-K.; Lehnert, N.; Neese, F.; Skulan, A. J.; Yang, Y.-S.; Zhou, J. Geometric and Electronic Structure/Function Correlations in Non-Heme Iron Enzymes. *Chem. Rev.* **2000**, *100*, 235−350.
(48) Whittaker, J. W.; Lipscomb, J. D.; Kent, T. A.; Münck, E. Brevibacterium Fuscum Protocatechuate 3,4-Dioxygenase. Purification, Crystallization, and Characterization. *J. Biol. Chem.* **1984**, *259*, 4466−4475.
(49) Bradley, F. C.; Lindstedt, S.; Lipscomb, J. D.; Que, L.; Roe, A. L.; Rundgren, M. 4-Hydroxyphenylpyruvate Dioxygenase Is an Iron-Tyrosinate Protein. *J. Biol. Chem.* **1986**, *261*, 11693−11696.
(50) Miller, M. A.; Lipscomb, J. D. Homoprotocatechuate 2,3-Dioxygenase from Brevibacterium fuscum. *J. Biol. Chem.* **1996**, *271*, 5524−5535.
(51) Taylor, S. W.; Chase, D. B.; Emptage, M. H.; Nelson, M. J.; Waite, J. H. Ferric Ion Complexes of a DOPA-Containing Adhesive Protein from Mytilus Edulis. *Inorg. Chem.* **1996**, *35*, 7572−7577.
(52) Liu, P.; Liu, A.; Yan, F.; Wolfe, M. D.; Lipscomb, J. D.; Liu, H. Biochemical and Spectroscopic Studies on (S)-2-Hydroxypropylphosphonic Acid Epoxidase: A Novel Mononuclear Non-Heme Iron Enzyme. *Biochemistry* **2003**, *42*, 11577−11586.
(53) Ormö, M.; deMaré, F.; Regnström, K.; Aberg, A.; Sahlin, M.; Ling, J.; Loehr, T. M.; Sanders-Loehr, J.; Sjöberg, B. M. Engineering of the Iron Site in Ribonucleotide Reductase to a Self-Hydroxylating Monooxygenase. *J. Biol. Chem.* **1992**, *267*, 8711−8714.
(54) Albe, K. R.; Butler, M. H.; Wright, B. E. Cellular Concentrations of Enzymes and Their Substrates. *J. Theor. Biol.* **1990**, *143*, 163−195.
(55) Price, J. C.; Barr, E. W.; Tirupati, B.; Bollinger, J. M.; Krebs, C. The First Direct Characterization of a High-Valent Iron Intermediate in the Reaction of an α-Ketoglutarate-Dependent Dioxygenase: A High-Spin Fe(IV) Complex in Taurine/α-Ketoglutarate Dioxygenase (TauD) from Escherichia coli. *Biochemistry* **2003**, *42*, 7497−7508.
(56) Matthews, M. L.; Chang, W.; Layne, A. P.; Miles, L. A.; Krebs, C.; Bollinger, J. M. Direct Nitration and Azidation of Aliphatic Carbons by an Iron-Dependent Halogenase. *Nat. Chem. Biol.* **2014**, *10*, 209−215.
(57) Yeh, E.; Kohli, R. M.; Bruner, S. D.; Walsh, C. T. Type II Thioesterase Restores Activity of a NRPS Module Stalled with an Aminoacyl-S-Enzyme That Cannot Be Elongated. *ChemBioChem* **2004**, *5*, 1290−1293.
(58) Wong, S. D.; Srnec, M.; Matthews, M. L.; Liu, L. V.; Kwak, Y.; Park, K.; Bell III, C. B., III; Alp, E. E.; Zhao, J.; Yoda, Y.; Kitao, S.; Seto, M.; Krebs, C.; Bollinger, J. M.; Solomon, E. I. Elucidation of the Fe(Iv)=O Intermediate in the Catalytic Cycle of the Halogenase SyrB2. *Nature* **2013**, *499*, 320−323.
(59) Srnec, M.; Wong, S. D.; Matthews, M. L.; Krebs, C.; Bollinger, J. M.; Solomon, E. I. Electronic Structure of the Ferryl Intermediate in the α-Ketoglutarate Dependent Non-Heme Iron Halogenase SyrB2: Contributions to H Atom Abstraction Reactivity. *J. Am. Chem. Soc.* **2016**, *138*, 5110−5122.
(60) Biswas, A. N.; Puri, M.; Meier, K. K.; Oloo, W. N.; Rohde, G. T.; Bominaar, E. L.; Münck, E.; Que, L. Modeling TauD-J: A High-Spin Nonheme Oxoiron(IV) Complex with High Reactivity toward C-H Bonds. *J. Am. Chem. Soc.* **2015**, *137*, 2428−2431.
(61) Krebs, C.; Galonić Fujimori, D.; Walsh, C. T.; Bollinger, J. M. Non-Heme Fe(IV)-Oxo Intermediates. *Acc. Chem. Res.* **2007**, *40*, 484−492.
(62) Srnec, M.; Iyer, S. R.; Dassama, L. M. K.; Park, K.; Wong, S. D.; Sutherlin, K. D.; Yoda, Y.; Kobayashi, Y.; Kurokuzu, M.; Saito, M.; Seto, M.; Krebs, C.; Bollinger, J. M.; Solomon, E. I. Nuclear Resonance Vibrational Spectroscopic Definition of the Facial Triad FeIV=O Intermediate in Taurine Dioxygenase: Evaluation of Structural Contributions to Hydrogen Atom Abstraction. *J. Am. Chem. Soc.* **2020**, *142*, 18886−18896.
(63) Davis, K. M.; Altmyer, M.; Martinie, R. J.; Schaperdoth, I.; Krebs, C.; Bollinger, J. M.; Boal, A. K. Structure of a Ferryl Mimic in the Archetypal Iron(II)- and 2-(Oxo)-Glutarate-Dependent Dioxygenase, TauD. *Biochemistry* **2019**, *58*, 4218−4223.
(64) Mehmood, R.; Vennelakanti, V.; Kulik, H. J. Spectroscopically Guided Simulations Reveal Distinct Strategies for Positioning Substrates to Achieve Selectivity in Nonheme Fe(II)/α-Ketoglutarate-Dependent Halogenases. *ACS Catal.* **2021**, *11*, 12394−12408.
(65) Farquhar, E. R.; Koehntop, K. D.; Emerson, J. P.; Que, L. Post-Translational Self-Hydroxylation: A Probe for Oxygen Activation Mechanisms in Non-Heme Iron Enzymes. *Biochem. Biophys. Res. Commun.* **2005**, *338*, 230−239.
(66) Chen, Y.-H.; Comeaux, L. M.; Herbst, R. W.; Saban, E.; Kennedy, D. C.; Maroney, M. J.; Knapp, M. J. Coordination Changes and Auto-Hydroxylation of FIH-1: Uncoupled O2-Activation in a Human Hypoxia Sensor. *J. Inorg. Biochem.* **2008**, *102*, 2120−2129.
(67) Zhao, C.; Yan, S.; Li, Q.; Zhu, H.; Zhong, Z.; Ye, Y.; Deng, Z.; Zhang, Y. An Fe 2+ - and α-Ketoglutarate-Dependent Halogenase Acts on Nucleotide Substrates. *Angew. Chem., Int. Ed.* **2020**, *59*, 9478−9484.
(68) Dai, L.; Zhang, X.; Hu, Y.; Shen, J.; Zhang, Q.; Zhang, L.; Min, J.; Chen, C.-C.; Liu, Y.; Huang, J.-W.; Guo, R.-T. Structural and Functional Insights into a Nonheme Iron- and α-Ketoglutarate-Dependent Halogenase That Catalyzes Chlorination of Nucleotide Substrates. *Appl. Environ. Microbiol.* **2022**, *88*, No. e02497.
(69) Neugebauer, M. E.; Kissman, E. N.; Marchand, J. A.; Pelton, J. G.; Sambold, N. A.; Millar, D. C.; Chang, M. C. Y. Reaction Pathway Engineering Converts a Radical Hydroxylase into a Halogenase. *Nat. Chem. Biol.* **2021**, *18*, 171−179.
(70) Goldberg, N. W.; Knight, A. M.; Zhang, R. K.; Arnold, F. H. Nitrene Transfer Catalyzed by a Non-Heme Iron Enzyme and Enhanced by Non-Native Small-Molecule Ligands. *J. Am. Chem. Soc.* **2019**, *141*, 19585−19588.
(71) Mitchell, A. J.; Dunham, N. P.; Bergman, J. A.; Wang, B.; Zhu, Q.; Chang, W.; Liu, X.; Boal, A. K. Structure-Guided Reprogramming of a Hydroxylase To Halogenate Its Small Molecule Substrate. *Biochemistry* **2017**, *56*, 441−444.
(72) Büchler, J.; Malca, S. H.; Patsch, D.; Voss, M.; Turner, N. J.; Bornscheuer, U. T.; Allemann, O.; Le Chapelain, C.; Lumbroso, A.; Loiseleur, O.; Buller, R. Algorithm-Aided Engineering of Aliphatic Halogenase WelO5* for the Asymmetric Late-Stage Functionalization of Soraphens. *Nat. Commun.* **2022**, *13*, 371.

https://doi.org/10.1021/acscatal.2c00954
ACS Catal. 2022, 12, 10913−10924